Modelling encapsulation tissue around cochlear implant electrodes

T. Hanekom

Department of Electrical, Electronic & Computer Engineering, University of Pretoria, Pretoria, South Africa

Abstract—*The objective of the study was to explore the effect of electrode encapsulation by fibrous scar tissue on electrical potential distributions and auditory nerve fibre excitation patterns. A finite element model in combination with an auditory nerve fibre model was used to predict changes in threshold currents and auditory nerve fibre excitation patterns. The model showed that electrical potentials at the target nerve fibres and the electrode contacts changed in the presence of encapsulation tissue. This led to changes in threshold currents and spread of excitation. The effect of electrode encapsulation on threshold currents and spread of excitation depended on the thickness of the perilymph layer separating the fibrous tissue encapsulation and the electrode array, nerve fibre survival status, electrode geometry and configuration, and array location. Model results suggested that arrays located close to the modiolus were most sensitive to threshold changes caused by electrode encapsulation (changes were between −0.26 and 2.41 dB), whereas encapsulation of an electrode array had less effect on threshold currents when the array was located in a lateral position in the scala tympani (changes were between −0.64 and 1.5 dB). For medially located arrays, changes in the spread of excitation varied between an increase of 0.21 mm and a decrease of 0.33 mm along the length of the basilar membrane, and an increase of 0.18 mm and a decrease of 0.66 mm along the length of the basilar membrane were calculated for laterally located arrays.*

Keywords—*Cochlear implants, Fibrous scar tissue, Thresholds, Neural excitation patterns, Finite element model*

Med. Biol. Eng. Comput., 2005, **43**, 47–55

1 Introduction

COCHLEAR IMPLANT subjects often experience changes in threshold current during the first few months after implantation. During one study, PFINGST (1990) reported that, in 88% of cases, thresholds were highest during a period some time during the first month after implantation and then decreased by 8–37 dB during the following weeks. EDDINGTON *et al.* (1988) and MILLER *et al.* (2000) also found threshold reduction over the first two to three months after surgery. PFINGST (1990) suggested that threshold reduction results from either changes in conductivity between the electrodes and the neural elements or changes in the sensitivity of the neural elements themselves. This study explores electrode encapsulation as a possible mechanism for causing threshold changes during the first few months after implantation.

Fibrous scar tissue and new bone often grow around intracochlear electrode arrays in animals and humans (LEAKE *et al.*, 1992; LINTHICUM *et al.*, 1991; WEBB *et al.*, 1988; ZAPPIA *et al.*, 1991). Tissue reaction to implanted materials can vary from toxic reactions (where inflammation and infection occur as a result of degradation of the implant material and/or implant orientation or geometry), to vital reactions, where the body detects the foreign object and incorporates it into the body by covering it in a vascularised fibrous scar tissue encapsulation (NANAS, 1988). Perfect biocompatibility does not exist in the true sense of the word (BERTOLUZZA *et al.*, 1992), as tissue reactions always occur to a greater or lesser extent at the biomaterial–tissue interface. Vital tissue reaction to intracochlear electrode arrays is thus the desired tissue response and also the most frequently observed response.

Tissue reactions to intracochlear electrode arrays range from very little fibrous tissue (LINTHICUM *et al.*, 1991; ZAPPIA *et al.*, 1991) to a dense, connective tissue cuff surrounded by loose, less dense tissue (ZAPPIA *et al.*, 1991) around the implant inside the scala tympani. New bone sometimes envelops the electrode array in the scala tympani of the basal turn (LINTHICUM *et al.*, 1991). GRILL and MORTIMER (1994) reported that the resistivity of encapsulation tissue is sufficient to alter the shape and magnitude of the electric field generated by chronically implanted electrodes. CLARK *et al.* (1995) also suggested that bone and fibrous tissue formation in the cochlea could account for variations in patients' speech perception. Changes in the tissues surrounding cochlear implant electrodes could thus affect the neural excitation patterns and

Correspondence should be addressed to Dr Tania Hanekom; email: tania.hanekom@eng.up.ac.za

Paper received 25 June 2003 and in final form 5 August 2004

MBEC online number: 20053959

therefore detection thresholds and dynamic ranges of electrical stimulation overall.

PFINGST (1990) found at most a weak correlation between implant impedances and threshold changes during the first months after implantation, whereas DE SAUVAGE *et al.* (1997) reported that compound action potential amplitudes and electrode impedance increased in correlation with each other. KAWANO *et al.* (1998) found that threshold T levels correlate with the presence of intracochlear fibrous tissue.

The objective of this study was to explore the effect of encapsulation tissue around cochlear implant electrodes on electrical potential distributions and auditory nerve fibre excitation patterns during electrical stimulation.

2 Model and methods

2.1 *Combined finite element–nerve fibre model*

A three-dimensional finite element (FE) model of the first one-and-a-half turns of the electrically stimulated cochlea was used to determine the effect of electrode encapsulation on the electrical potential distributions and thus neural excitation patterns during electrical stimulation. The cochlear model was created by first creating the geometry of a transverse plane through the cochlea in an FE software environment. This two-dimensional geometry is shown in Fig. 1*a*. The two-dimensional geometry was then extruded into three dimensions around the axis of the modiolus (Fig. 1*b*). The diameters of the structures were not tapered towards the apical end of the model. For this study, the effect of the untapered nature of the model was negligible, as electrodes in an electrode pair were usually closely spaced. The modelled cochlea was embedded into a cylinder consisting of bone elements. The location of the bone cylinder is shown by broken lines in Fig. 1*b*.

The axons were extended so that the nerve fibres originating from the upper half-turn of the model extended downwards to at least below the scala tympani of the lower half-turn of the model. To be a true representation of the anatomy, the axons should combine into one nerve bundle. In the model, this was realised by 'filling' the volume enclosed by the medial axonal processes with nerve tissue, i.e. setting the material properties of elements in this volume to that of nerve tissue. The volume of nerve tissue extended to the end of the bone cylinder, thereby creating a low conductance path along the modiolus. Fig. 1*b* does not show the nerve tissue enclosed by the medial axonal processes (which are protruding below the scalae).

The materials in the model were purely resistive, because it has been shown that, to a first approximation, cochlear tissue impedances are well approximated by pure resistances (BLACK *et al.*, 1981; SPELMAN *et al.*, 1980; 1982). This assumption implies undistorted propagation of the excitation waveform and allows the field calculation to be treated as a steady-state conduction problem (FINLEY *et al.*, 1990). The reader is referred to the paper by HANEKOM (2001) for further details about the model.

The encapsulation tissue was modelled as a material layer with a resistivity of 627 Ω-cm around the electrode array. The resistivity of the encapsulation tissue was based on the measurements by GRILL and MORTIMER (1994) on encapsulation tissue around electrodes implanted subcutaneously in cats. In the FE model, an encapsulation tissue thickness of 50 μm was used, based on observations of an average intracochlear fibrous tissue thickness around silastic electrode carriers of 48.5 μm (SELDON *et al.*, 1994) and to allow two electrode arrays surrounded by encapsulation tissue to fit within the scala tympani (i.e. to allow two electrode array locations). Simulation results were generated for three encapsulation

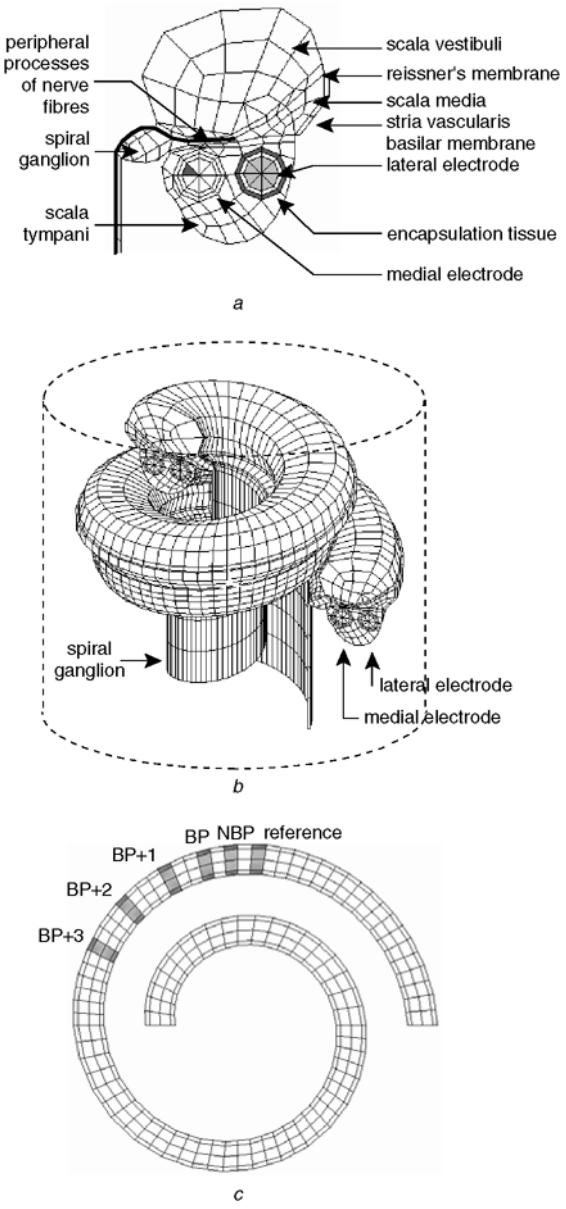

Fig. 1 *(a) Two-dimensional plane through one turn of FE cochlear model to show two array locations and location of encapsulation tissue. Bold line shows location of neural sheet on which electrical potential distribution was calculated to determine thresholds and neural excitation patterns. (b) Oblique view of three-dimensional geometry of cochlear model. (– – –) Outlines of bone cylinder in which cochlear model is embedded. Nerve tissue in modiolus is not shown. (c) Top view of one of modelled electrode arrays showing various electrode configurations*

variations: an electrode without encapsulation tissue (called 'clean'), an electrode array surrounded by a 50 μm layer of encapsulation tissue in direct contact with the electrode carrier (direct encapsulation (DE)) and an electrode array surrounded by a 50 μm layer of encapsulation tissue separated from the electrode carrier by a 50 μm layer of perilymph (separated encapsulation (SE)).

Two electrode arrays (using banded or point electrode contacts) and two array locations (one medial and one lateral in the scala tympani relative to the modiolus) were modelled. Banded electrode contacts refer to contacts that are formed by rings that are located on the surface of the electrode carrier. Point electrode contacts is a general term to refer to small disc- or ball-shaped or square-planar electrode contact geometries. The banded array at a medial location in the

scala tympani was called banded medial (BM), and the array at a more lateral location in the scala tympani was called banded lateral (BL). Likewise, the point electrode arrays were called point medial (PM) and point lateral (PL). The locations of the medial and lateral electrode arrays are shown in Figs 1*a* and *b*. The contacts of the point electrode arrays were in a medial-superior orientation. The radial orientation of the elements in the modelled electrode array that were used to create the point electrodes is indicated by a shaded element (triangle) in the medial electrode array on the two-dimensional plane through the model (Fig. 1*a*).

Only one array existed during a specific simulation. An array was selected by the material properties of its elements being changed to those of an insulator or a conductor, and the material properties of the other array were changed to that of perilymph. In Fig. 1*a*, it can be seen that an electrode array in the model consisted of a core and two layers around it. The core was defined as the electrode carrier (elements in lateral electrode array lightly shaded in Fig. 1*a*), i.e. the resistivity of the elements in these components was set to that of an insulator). The electrode contacts were defined on the surface of the core by defining banded or point equipotential surfaces and applying the stimulation current to these surfaces.

The first layer surrounding the core was used to define either the encapsulation tissue for the DE case or the layer of perilymph separating the electrode array and the encapsulation tissue for the SE case. The second layer of elements around the core (i.e. the layer not directly in contact with the core) was used to define the encapsulation tissue (darkly shaded in Fig. 1*a*) for the SE case.

Six electrode configurations were modelled. Details of the electrode configurations are listed in Table 1, and their locations in the model are shown in Fig. 1*c*.

Table 1 Details of electrode configurations in FE model

Abbreviation	Description of electrode configuration	Electrode separation*, mm
NBP	near bipolar, longitudinal bipolar configuration with electrode separation approximately half the separation between neighbouring electrodes in Nucleus cochlear implant (CLARK, 1996)	0.29
BP	bipolar refers to electrode configuration consisting of two neighbouring electrodes in Nucleus cochlear implant	0.83
BP+1	bipolar plus 1: electrode configuration consisting of two electrodes separated with one electrode in Nucleus cochlear implant	1.65
BP+2	bipolar plus 2: similar to BP+1	2.72
BP+3	bipolar plus 3: similar to BP+1	3.78
MONO	monopolar mode where return electrode is located outside scala tympani at remote site	not applicable

*Model geometry only allows for approximate electrode separations relative to electrode separations for Nucleus electrode array (HANEKOM, 2001)

Electrical potential distributions generated by electrical stimulation with a 200 μA DC current were calculated on a plane in the model (HANEKOM, 2001) containing the auditory nerve fibres. A section through the neural plane is indicated with a bold line in Fig. 1*a*.

2.2 *Modelling of auditory nerve fibre excitation*

The FE model of the cochlea consisted of 90 segments (Fig. 1*c*). Electrical potentials were calculated on the boundaries of the segments, producing 91 sets of potential values. Consequently, 91 nerve fibres (forming a nerve fibre array) were modelled. If a uniform nerve fibre density of 13 600 nerve fibres per cochlear turn (calculated from SPOENDLIN and SCHROTT (1989), based on a cochlear length of 30 mm) was assumed throughout the modelled cochlea, each modelled nerve fibre represented approximately 224 real nerve fibres.

Thresholds were determined with the generalised Schwarz–Eikhof–Frijns (SEF) auditory nerve fibre model (FRIJNS *et al.*, 1995). Two types of nerve survival were modelled: one where the nerve fibres were intact and thus included the peripheral dendrites (as would be expected for implantees with significant residual hearing and/or relatively short duration of deafness) and another where the peripheral dendrites of the nerve fibres had degenerated (as would be expected after a long period of deafness). To simulate loss of peripheral dendrites after a long period of deafness, a truncated version of the generalised SEF model (FRIJNS *et al.*, 1996; HANEKOM, 2001) was used.

The stimulus was a 200 μs per phase, charge-balanced, biphasic current pulse. Although electrical potential distributions calculated with the FE model were generated with a 200 μA DC stimulus, biphasic stimuli with any amplitude could be created by scaling because of the resistive nature of the FE model (HANEKOM, 2001). The threshold current for a nerve fibre was defined as the lowest current level that excited the nerve fibre during a single stimulation cycle. Nerve excitation was assumed when a propagating action potential occurred (REILLY *et al.*, 1985). The occurrence of an action potential was detected by an iterative process. An interval was defined in which the threshold current was expected to occur. The current level was then stepped down or up by halving of the interval with each iteration, depending on whether the current level caused an action potential or not. The final resolution of the iterative process was 1 μA.

3 Results

Fig. 2*a* shows representative results for potential distributions generated by the finite element model, and Fig. 2*b* shows representative results for neural excitation patterns obtained with the combined FE–nerve fibre model. Potential distributions for bipolar electrode configurations always exhibit a maximum and a minimum, as shown in Fig. 2*a*, corresponding to the polarity of the electrode located at the specific position. In Fig. 2*a*, the locations of the electrodes along the length of the basilar membrane are indicated with two blocks at the top of the Figure. Horizontal dotted lines indicate the location of the nodes in the nerve fibre model, and vertical dotted lines indicate the boundaries between the first and second, and second and third half-turns of the finite element model. Potential distributions for a monopolar electrode configuration only exhibit a minimum or a maximum, depending on the polarity of the active electrode.

The reference (0 dB) for the graphs in Fig. 2*b* was taken as the minimum threshold current intensity that evoked a response (reported in Fig. 3), to facilitate comparison of spread of excitation for various electrode configurations, geometries and

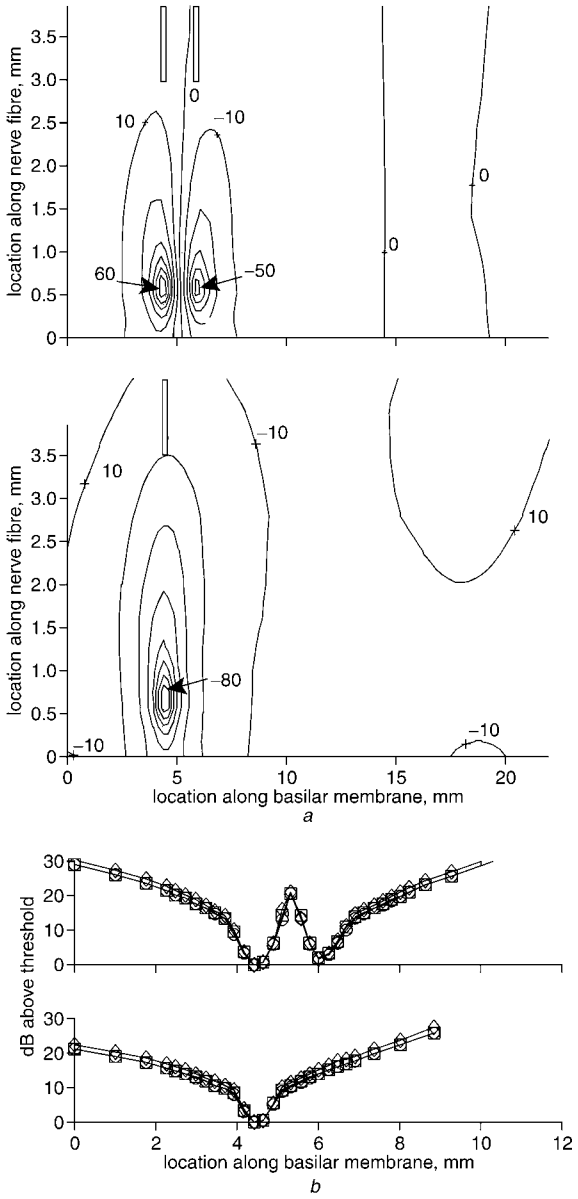

Fig. 2 *(a) Potential distribution for PM array for BP+1 (upper graph) and MONO (lower graph) electrode configurations with direct encapsulation. (b) Neural excitation patterns calculated with combined FE-nerve fibre model for PM electrode array using full nerve fibre model (i.e. peripheral process of fibre is intact). (—□—) Clean; (—◇—) DE; (—○—) SE. Upper graph shows bimodal excitation pattern generated with BP+1 electrode configuration; lower graph shows unimodal excitation pattern generated with monopolar electrode configuration*

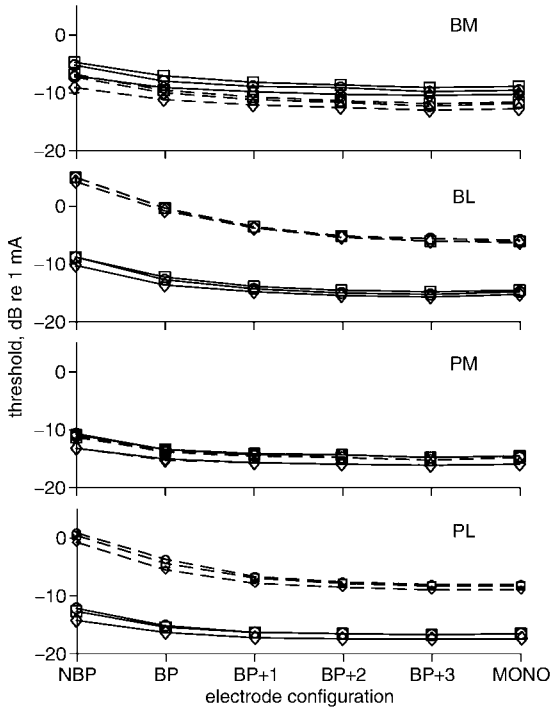

Fig. 3 *Threshold current as function of electrode configuration. (—□—) Clean; F-fibre; (—◇—) DE: F-fibre; (—○—) SE: F-fibre. (□) Clean: T-fibre; (—◇—) DE: T-fibre; (—○—) SE: T-fibre*

array locations at a specific stimulation intensity above threshold. The graphs were generated by calculation of the stimulus intensity that had to be presented by an electrode pair to activate each nerve fibre in the nerve fibre array and then subtraction of the minimum threshold (Fig. 3) from the result for the specific electrode geometry, location or configuration.

The upper graph is for the BP+1 electrode configuration, and the lower graph is for monopolar electrode configuration for the PM array. All the bipolar electrode configurations create bimodal excitation patterns, because excitation occurs at both electrode contacts in an electrode pair. This is because of biphasic (but opposite in polarity) stimuli that are presented on both contacts in an electrode pair during a single stimulation period (FRIJNS *et al.*, 1996; HANEKOM, 2001). Monopolar configurations elicit a unimodal excitation pattern, as the return electrode is located remotely, outside the scala tympani. Excitation patterns are localised around the location of the electrode contacts at lower stimulus intensities. This localisation generally occurs up to higher stimulus intensities for bipolar electrode configurations than for monopolar configurations (HANEKOM, 2001).

Fig. 3 summarises threshold current intensities as a function of electrode configuration. Thresholds are affected by electrode configuration, electrode geometry, array location, state of the nerve fibre (i.e. whether the full nerve fibre model or the truncated nerve fibre model has been used) and the presence or absence of encapsulation tissue.

Threshold differences caused by variations in electrode configuration, electrode geometry, array location and the state of the nerve fibre have been dealt with in a previous paper (HANEKOM, 2001). To summarise: thresholds tend to be lower when the electrode array is close to the fibre terminals, i.e. lower thresholds will usually be observed for the BL array when a full nerve fibre model is used, rather than when the truncated nerve fibre model is used. The effect is less pronounced for electrode arrays that are located in a medial location in the scala tympani.

Widely spaced electrode configurations cause lower threshold currents than narrowly spaced electrode configurations. This is because the potential at the target nerve fibres increases with increasing inter-electrode separation (Fig. 4). Arrays close to the modiolus cause a decrease in thresholds, because the target nerve fibres are in close proximity to the stimulating source points and thus require less current to be activated. Point electrode geometries have lower thresholds than banded electrode geometries if the electrode contacts are oriented towards the residual nerve elements. This is because point electrodes force the current distribution toward the target nerve fibres. Banded electrodes distribute the current radially around the electrode carrier (including

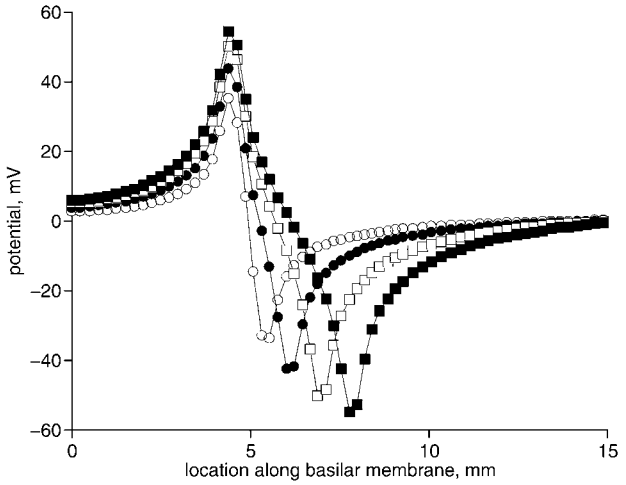

Fig. 4 *Maximum potential deviation for various inter-electrode separations along fifth node of neural model, i.e. 0.503 mm on ordinate of Fig. 2a. This result is for BM electrode array for DE case. Trend shown in these results, i.e. increase in maximum potential deviation with increasing inter-electrode separation, is similar for all modelled array locations, electrode geometries and encapsulation types. (—○—) BP; (—●—) BP+1; (—□—) BP+2; (—■—) BP+3*

regions where no nerve fibres are present) and are thus less effective than point electrodes.

Table 2 summarises the threshold difference between the clean electrode arrays and the DE and SE cases. A positive value means that the threshold for the clean case is higher than for the encapsulated case and that the encapsulation causes a reduction in the threshold current. Both point and banded electrode geometries generally exhibit substantial threshold reductions for the DE case, using either the full or truncated nerve fibre model. For the SE case, threshold reduction is less, but still present in most cases. For the lateral electrode array locations using the truncated nerve fibre model, thresholds are either influenced very little or increased relative to those of the clean arrays. Threshold reduction is higher for arrays close to the modiolus (i.e. BM and PM arrays) than for arrays at a more lateral location.

Fig. 2*b* shows that the presence of direct encapsulation around a PM electrode array decreases the spread of excitation, especially at higher stimulus intensities. For separated encapsulation, no effect is visible from these graphs. To evaluate the effect of encapsulation tissue on the localisation of activation, spread of excitation along the basilar membrane at 10 dB above threshold was plotted as a function of electrode separation (Fig. 5). Spread of excitation along the basilar membrane is presented, in millimetres, and was determined by calculating the total region of excitation, excluding the non-excited region in between excited regions in the case of bimodal excitation patterns, using an interpolation method. The graphs show that threshold changes associated with electrode encapsulation do occur. These changes vary from very little (BL array) to pronounced (BM array with the full nerve fibre model).

Table 2 summarises the difference in 10 dB spread of excitation between the clean arrays and DE and SE arrays. A positive value indicates a reduction in the spread of excitation, i.e.

Table 2 Threshold difference, in dB, relative to control electrode array and change in spread of excitation, in mm, relative to control electrode array

Electrode configuration		Threshold difference for clean electrode, dB				Difference in spread of excitation for clean electrode, mm			
		F-fibre		T-fibre		F-fibre		T-fibre	
		DE	SE	DE	SE	DE	SE	DE	SE
NBP	BM	2.41	0.53	2.27	0.33	0.12	−0.09	0.18	−0.06
	BL	1.41	0.05	0.60	−0.07	0.10	−0.06	0.03	0.00
	PM	2.41	−0.26	1.88	−0.18	0.02	−0.09	0.08	−0.09
	PL	1.51	−0.50	1.22	−0.59	0.09	−0.14	0.16	−0.09
BP	BM	2.03	0.84	1.72	0.51	0.03	−0.05	0.04	−0.03
	BL	1.26	0.39	0.51	0.02	0.05	−0.21	−0.01	0.01
	PM	1.76	0.00	1.59	0.16	−0.01	−0.07	−0.09	−0.16
	PL	1.11	−0.10	1.19	−0.64	0.01	−0.10	0.22	−0.17
BP+1	BM	1.73	0.81	1.31	0.44	0.32	0.03	0.25	0.00
	BL	0.98	0.52	0.39	0.28	0.10	0.01	0.03	0.02
	PM	1.55	0.04	1.29	0.22	0.06	−0.11	0.12	−0.08
	PL	0.95	0.06	0.88	−0.39	0.14	−0.13	0.18	−0.13
BP+2	BM	1.74	0.70	1.29	0.40	0.67	0.18	0.37	0.05
	BL	0.86	0.32	0.17	−0.21	0.18	0.06	0.06	0.03
	PM	1.57	0.04	1.23	0.14	0.12	−0.12	0.18	−0.10
	PL	0.85	0.00	0.79	−0.36	0.18	−0.17	0.19	−0.14
BP+3	BM	1.37	0.67	1.03	0.35	0.62	0.26	0.33	0.06
	BL	0.83	0.38	0.07	−0.29	0.22	0.04	0.16	0.07
	PM	1.46	0.00	1.08	0.10	0.12	−0.15	0.21	−0.09
	PL	0.86	0.06	0.76	−0.34	0.22	−0.14	0.22	−0.14
MONO	BM	1.38	0.61	1.04	0.24	0.66	0.26	0.40	0.01
	BL	0.76	0.28	0.18	−0.23	0.14	0.01	0.16	−0.07
	PM	1.48	0.05	1.14	0.05	0.33	−0.04	0.21	−0.05
	PL	0.85	0.00	0.72	−0.34	0.13	−0.08	0.33	−0.18
Average	BM	1.78	0.69	1.44	0.38	0.40	0.10	0.26	0.01
	BL	1.02	0.32	0.32	−0.08	0.13	−0.03	0.07	0.01
	PM	1.71	−0.02	1.37	0.08	0.11	−0.10	0.12	−0.10
	PL	1.02	−0.08	0.93	−0.44	0.13	−0.13	0.22	−0.14

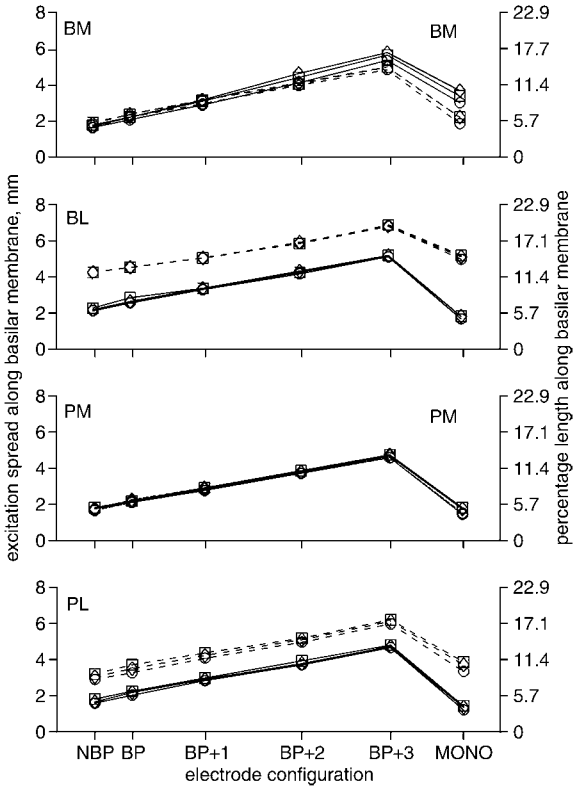

Fig. 5 *Spread of excitation along length of basilar membrane as function of electrode configuration at stimulus intensity of 10 dB above threshold. Locations of electrode configurations on abscissa have been scaled to represent their respective inter-electrode separations in FE model, except for monopolar electrode configuration. (—○—) DE: F-fibre; (—□—) SE: F-fibre; (—◇—) clean: F-fibre. (—○—) DE: T-fibre; (—□—) SE: T-fibre: (—◇—) clean: T-fibre*

the spread of excitation for the encapsulated array is less than that for the clean array. Spread of excitation is generally decreased for the DE case. For the BM electrode array with widely spaced electrode configurations (including monopolar configuration), the reduction is more than 0.6 mm. For the other electrode geometries and locations, the reduction for the DE case is approximately 0.1–0.2 mm.

For the SE case, spread of excitation is reduced for the BM electrode array when widely spaced electrode configurations are used (i.e. larger than BP+1). For this electrode array, the reduction is close to zero when the truncated nerve fibre model is used. For closely spaced electrode configurations and for the BL and point electrode arrays, spread of excitation is either nearly unchanged or increased by the presence of encapsulation tissue.

4 Discussion

4.1 *Threshold variations*

The changes in threshold currents can be explained by examining the effect of encapsulation tissue on the maximum potential deviation (Fig. 6*a*), which occurs on a line through the fifth node of the neural models (0.503 mm on the ordinate of Fig. 2*a*). Fig. 6*a* shows that the DE case has the highest potential deviation, followed by the SE and then the clean cases. The potential increase at the target nerve fibres results from an increase in the current density at the fibres, because of a relative narrowing of the electric field, i.e. the width of the field deviation remains virtually constant, but the magnitude of the field increases (Fig. 6*b*).

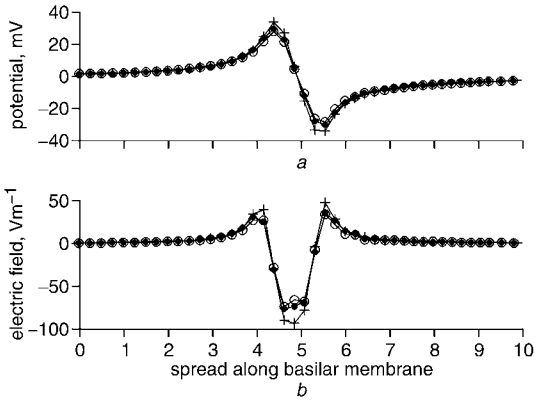

Fig. 6 *(a) Maximum potential deviation and (b) electric field distribution for different types of encapsulation along fifth node of neural model, i.e. 0.503 mm on ordinate of Fig. 2a. These results are for BM electrode array. Trend shown in results, i.e. highest potential deviation and electric field intensity for (+) DE case, followed by (—•—) SE and then (—○—) clean cases is similar for all modelled array locations and electrode geometries*

It should be noted, at this stage, that the level of correlation between implant impedance and threshold current changes probably does not reflect the status of the encapsulation tissue layer, as the relatively high electrode–body fluid interface impedance, i.e. 10–20 kΩ (DE SAUVAGE *et al.*, 1997; DORMAN *et al.*, 1992), dominates resistive changes caused by encapsulation tissue (roughly hundreds of ohms) in the neighbouring cochlear tissue.

The variability of the effect of scar tissue can be seen from the study by KAWANO *et al.* (1998). They performed post-mortem examinations of five human, implanted cochleas and statistically correlated psychophysical parameters with intracochlear pathology. Temporal bones used in the study were from donors who had received Nucleus 22-channel cochlear implants. KAWANO *et al.* (1998) found significant positive correlation between psychophysical threshold levels (T-levels) and the occurrence of fibrous scar tissue around the electrode array in two of the five cases, no significant correlation in two cases and significant negative correlation in one case. The data measured by KAWANO *et al.* (1998) correspond to the modelled BL electrode array, as this is the normal location for the straight Nucleus 22 electrode array (SHEPHERD *et al.*, 1993).

Threshold changes for the BL array vary from a decrease of 1.26 dB for the BP electrode configuration (the NBP configuration with a decrease of 1.41 dB is not clinically relevant), using the full nerve fibre model with direct encapsulation, to an increase of 0.29 dB for the BP+3 electrode configuration, using the truncated nerve fibre model and separated encapsulation. The model therefore accounts for the observed variations in the correlation between T-levels and the occurrence of fibrous tissue by including variations in the thickness of the perilymph layer separating the electrode array and the encapsulation tissue, as well as variations in nerve fibre survival status, i.e. the extent to which the peripheral dendrites have degenerated. From the results, it is also evident that electrode configuration and separation and array location influence the effect of electrode encapsulation on threshold current levels.

For array locations far from the target nerve fibres and widely spaced electrode configurations, the effect of encapsulation tissue on threshold currents is limited by greater volumes of cochlear tissue between the electrodes and the target nerve fibres. We would therefore expect to see more

pronounced threshold current variations because of electrode encapsulation for implants with arrays close to the modiolus, e.g. the Clarion (KESSLER, 1999; YOUNG and GROHNE, 2001) cochlear implant, than for implants with arrays far from the modiolus, e.g. the Nucleus (CLARK, 1996) cochlear implant. This is evident from the data presented in Table 2, where threshold variations for medial arrays are generally greater than for lateral arrays. Some evidence supporting this observation can be found in threshold current reductions over time, reported by PFINGST (1990) (who used arrays that positioned electrode contacts in the region between the modiolus and the middle of the scala tympani) and DORMAN *et al.* (1992) (for patients using the Ineraid cochlear implant), whereas unchanged EABR thresholds over time were reported for Nucleus implant users (BROWN *et al.*, 1995).

Threshold current reductions predicted by the model that could be compared with the data of PFINGST (1990) are most likely those observed for the full nerve fibre model, as primate subjects were either deafened during implantation or not deafened at all. A further assumption would be that the implanted arrays were either similar to the PM array (multichannel implants used in the study) or the BM array (single spherical electrodes introduced into the scala tympani). Threshold reductions for these conditions range between 1.38 dB and 2.03 dB for clinically employed electrode configurations (i.e. excluding the NBP electrode configuration) for the DE case and between 0 dB and 0.84 dB for the SE case. Threshold changes can be translated to rates of threshold reduction by dividing the reduction in threshold as a result of electrode encapsulation by a time period (25 days to be comparable with the data measured by PFINGST (1990)). Threshold reductions predicted by the model therefore range between 0.055 and 0.081 dB per day for the DE case and between 0 and 0.034 dB per day for the SE case. Electrode encapsulation could thus account only partly for the observed threshold current reductions of 0.2–1 dB per day reported by PFINGST (1990).

Variations in thresholds for the NBP electrode configuration as a result of encapsulation tissue are more pronounced than for wider electrode configurations. This could mean that high-density electrode arrays (JOLLY *et al.*, 1997; SPELMAN *et al.*, 1996), which have been proposed as a new-generation alternative to current electrode arrays, could be more susceptible to threshold changes as a result of electrode encapsulation. Also, as such an electrode array would probably be located in a perimodiolar position (the new-generation electrode arrays are designed to fit snugly around the modiolus (BALKANY *et al.*, 2002; GSTOETTNER *et al.*, 2001)), the additional threshold variations associated with arrays close to the modiolus could add to this effect.

4.2 *Spread of excitation*

COHEN *et al.* (2003) calculated spread of excitation as a percentage along the length of the organ of Corti for monopolar stimulation with the Nucleus 24 banded (or 'straight') electrode array and for the Nucleus 24 Contour array. Monopolar stimulation with the BL array could be compared with the results obtained for the Nucleus 24 banded array, and the results for the Contour array can be expected to be somewhere between those for the modelled BM and PM arrays, as the Contour array has half-bands instead of point or banded electrode geometries, and its location is usually closer to the modiolus than that of the straight banded electrode array. However, there is no direct relationship between the simulated decibels above threshold levels and loudness levels as used in the study by COHEN *et al.* (2003). Nevertheless, if an average cochlear duct length of 35 mm (SKINNER *et al.*, 1994) is used, the modelled results, given in units of millimetres along the basilar membrane (left axes in Fig. 5), could be translated to units of percentage length along the basilar membrane (right axes in Fig. 5).

Two comparisons can be made between the modelled data presented in this study and the measured data of COHEN *et al.*: it was found that spread of excitation was similar for BP+1 and MONO electrode configurations (COHEN *et al.*, 2001), which is also true for the BM array as well as for the BL and PL arrays using the truncated nerve fibre model; and, secondly, spread of excitation was overall narrower for the Contour array than for the straight array (COHEN *et al.*, 2003), which is also the case for the modelled results (compare results for lateral and medial array locations in Fig. 5) using the truncated nerve fibre model.

Unfortunately, the data presented by COHEN *et al.* (2003) were measured mostly at 50% and 80% loudness levels, which could be louder than the 10 dB above threshold levels at which spread of excitation was evaluated for this study. This remark is based on the observation that spread of excitation predicted by the model is generally less than the measured results. However, spread of excitation at 20% loudness intensity for one subject using monopolar stimulation with a straight banded electrode array (at electrode 10) is approximately 15% of the basilar membrane length, which is roughly equivalent to the 14% of the basilar membrane length predicted by the model for the BL array using the truncated nerve fibre model.

Spatial spread of excitation, as recently evaluated by a number of researchers (COHEN *et al.*, 2001; 2003; FRIJNS *et al.*, 2002), further suggested that, although spread of excitation was typically restricted to nerve fibres in the vicinity of the stimulation site, there was not always correlation between electrode-to-modiolus proximity and spread of excitation, and considerable inter-person and inter-electrode variability occurred. This variability in spread of excitation could partly be ascribed to the influence of encapsulation tissue on spread of excitation.

BROWN *et al.* (1995) reported a slight but significant reduction in EABR slope with time for subjects implanted with the Ineraid implant. EABR slope gives an indication of the increase or decrease in the number of excited nerve fibres. EABR slope can thus be interpreted as a measure of spread of excitation and dynamic range, i.e. a shallower EABR slope corresponds to a narrower region of excitation (a slow increase in the number of excited nerve fibres with increasing stimulation current) and a larger dynamic range (FRIJNS *et al.*, 1995). Model results suggest that spread of excitation is typically limited by the presence of encapsulation tissue (Fig. 5 and Table 2) if the encapsulation resembles the DE case. This suggests that dynamic range could be increased by the presence of encapsulation tissue in direct contact with the electrode array. However, when the encapsulation is separated from the electrode array by a perilymph layer, the changes in spread of excitation generally become a function of electrode geometry and electrode configuration. Spread of excitation is typically decreased for banded electrode arrays, especially for widely spaced electrode configurations. However, for point electrode arrays, spread of excitation is invariably increased.

Changes in spread of excitation as a result of electrode encapsulation seem small (less than 0.5 mm in most cases), but they cannot be ignored. The neural resolution of the model is rough, i.e. each modelled nerve fibre represents approximately 224 real nerve fibres or, in other words, only every 224th nerve fibre in the cochlea is included in the model. A rough approximation could be made, based on the findings of SPOENDLIN and SCHROTT (1989), which indicate a hair cell density of approximately 100 inner hair cells

per millimetre along the basilar membrane. If the nerve fibres connecting to each hair cell were located next to the inner hair cells and the hair cells were spaced regularly in a line along the length of the basilar membrane (a reasonable assumption based on the anatomy of the organ of Corti as reported by ENGSTRÖM *et al.* (1970)), the nerve fibres of each inner hair cell would be spaced at 0.01 mm intervals along the length of the basilar membrane. This is also roughly consistent with the 9 μm hair cell thickness reported by ZWICKER and FASTL (1990). Noticeable but small variations in the calculated spread of excitation could thus amount to a significant number of nerve fibres for which the threshold current of an electrode pair has changed. The smallest variations shown in Table 2 are 0.01 mm, which amounts to the nerve fibres of approximately one inner hair cell for which the threshold currents have changed. This would be equivalent to about three–four fibres per inner hair cell in the basal and apical parts of the cochlea and up to 15 fibres per inner hair cell in the lower second turn of the cochlea (SPOENDLIN and SCHROTT, 1989).

4.3 *Clinical implications*

The effect of electrode encapsulation is somewhat unpredictable, as the parameters that influence its effect are not necessarily known. Looking at average values for variations in threshold currents and spread of excitation it seems as though electrode encapsulation is beneficial if the encapsulation resembles the DE case, with reductions in both thresholds and spread of excitation for both banded and point electrode geometries and both medial and lateral array locations. For the SE case, the potential benefit becomes a function mainly of electrode geometry, but also of nerve fibre survival. Threshold current reductions are generally observed for banded arrays, except for the BL array when the T-fibre is used. Spread of excitation is also reduced for banded arrays, except for the BM array when the full nerve fibre model is used. The model thus predicts that electrode encapsulation could be beneficial for the BM array using the T-fibre model and for the BL array using the F-fibre model when SE occurs and partly beneficial for the other two cases.

In summary, model results suggest that electrode encapsulation would normally not be detrimental to threshold current levels and spread of excitation if banded electrode arrays are used and could, in most cases, be beneficial. However, if point electrode geometries are used, no benefits are generally obtained from electrode encapsulation and, if possible, measures should be employed to reduce fibrous tissue formation around such arrays.

The implication is that cochlear implants employing arrays located close to the modiolus, such as the Nucleus Contour (TYKOCINSKI *et al.*, 2001) or Clarion HiFocus (which was recently withdrawn from the market) electrode arrays, are most sensitive to threshold changes caused by electrode encapsulation, whereas encapsulation of an electrode array has less effect on threshold currents when the array is located in a lateral position in the scala tympani, such as the standard, straight Nucleus 22 or 24 electrode arrays.

Model results also suggest that threshold currents and spread of excitation of implants using high-density electrode arrays implementing closely spaced bipolar stimulation (similar to the NBP electrode configurations) are more likely to be affected by electrode encapsulation than lower density arrays such as those currently employed in commercial cochlear implants.

5 Conclusions

Results presented in this article suggest that electrode encapsulation can alter threshold currents and spread of excitation. The effect of electrode encapsulation on threshold currents depends, in the first place, on the thickness of the perilymph layer separating the electrode array and the encapsulation layer. If the encapsulation is in direct contact with the electrode array, significant threshold reductions occur for all electrode geometries and array locations, whatever the nerve fibre model (full or truncated) used. However, if the encapsulation tissue is separated from the electrode array by a perilymph layer (with a thickness equal to that of the encapsulation tissue layer in this article), threshold reductions are either small (less than 1 dB) or increased relative to those for a clean array.

Part of the decreases in threshold currents observed by PFINGST (1990) during the first few months after implantation could be accounted for by electrode encapsulation. However, other mechanisms, such as sensitisation for electrical stimulation (TYE-MURRAY *et al.*, 1992), are likely to have a more significant effect on the observed threshold reduction than electrode encapsulation.

Variations in spread of excitation are also strongly dependent on the presence or absence of a perilymph layer between the electrode array and the encapsulation tissue and are mostly reduced when direct encapsulation of the array occurs. This could be beneficial, as a reduction in the spread of excitation could increase dynamic range. Spread of excitation is either increased (point electrode geometries) or affected very little by separated encapsulation of the electrode array.

Model results suggest that arrays located close to the modiolus, such as the Nucleus Contour or Clarion HiFocus electrode arrays, are most sensitive to threshold changes caused by electrode encapsulation, whereas encapsulation of an electrode array has less effect on threshold currents when the array is located in a lateral position in the scala tympani, such as the standard, straight Nucleus 22 or 24 electrode arrays.

Further studies should include a detailed investigation of the effect of the thickness of the perilymph layer separating the electrode and fibrous tissue encapsulation. The optimum separation distance between encapsulation and electrode, i.e. the separation distance at which encapsulation generally becomes beneficial, could be estimated to provide a measure by which the effect of electrode encapsulation could be predicted for a specific person.

Acknowledgment—The author wishes to thank Michelle Joubert for running many of the simulations required to generate the data presented in this study.

References

BALKANY, T. J., ESHRAGHI, A. A., and YANG, N. (2002): 'Modiolar proximity of three perimodiolar cochlear implant electrodes', *Acta Otolaryngologica*, **122**, pp. 363–369

BERTOLUZZA, A., FAGNANO, C., MONTI, P., SIMONI, R., TINTI, A., TOSI, M. R., and CARAMAZZA, R. (1992): 'Raman spectroscopy in the study of biocompatibility', *Clin. Mater.*, **9**, pp. 49–68

BLACK, R. C., CLARK, G. M., and PATRICK, J. F. (1981): 'Current distribution measurements within the human cochlea', *IEEE Trans. Biomed. Eng.*, **28**, pp. 721–724

BROWN, C. J., ABBAS, P. J., BERTSCHY, M., TYLER, R. S., LOWDER, M., TAKAHASHI, G., PURDY, S., and GANTZ, B. J. (1995): 'Longitudinal assessment of physiological and psychophysical measures in cochlear implant users', *Ear Hearing*, **16**, pp. 439–449

CLARK, G. M., SHUTE, S. A., SHEPHERD, R. K., and CARTER, T. D. (1995): 'Cochlear implantation: Osteoneogenesis, electrode-tissue impedance, and residual hearing', *Ann. Otol., Rhinol. Laryngol. Suppl. (United States)*, **166**, pp. 40–42

CLARK, G. M. (1996): 'Electrical stimulation of the auditory nerve: the coding of frequency, the perception of pitch and the development of cochlear implant speech processing strategies for profoundly deaf people', *Clin. Exp. Pharmacol. Physiol.*, **23**, pp. 766–776

COHEN, L. T., SAUNDERS, E., and CLARK, G. M. (2001): 'Psychophysics of a prototype peri-modiolar cochlear implant electrode array', *Hearing Res.*, **155**, pp. 63–81

COHEN, L. T., RICHARDSON, L. M., SAUNDERS, E., and COWAN, R. S. (2003): 'Spatial spread of neural excitation in cochlear implant recipients: comparison of improved ECAP method and psychophysical forward masking', *Hearing Res.*, **179**, pp. 72–87

DE SAUVAGE, R. C., DA COSTA, D. L., ERRE, J.-P., and ARAN, J. M. (1997): 'Electrical and physiological changes during short-term and chronic electrical stimulation of the normal cochlea', *Hearing Res.*, **110**, pp. 119–134

DORMAN, M. F., SMITH, L. M., DANKOWSKI, K., MCCANDLESS, G., and PARKIN, J. L. (1992): 'Long-term measures of electrode impedance and auditory thresholds for the Ineraid cochlear implant', *J. Speech Hearing*, **35**, pp. 1126–1130

EDDINGTON, D., DOBELLE, W., BRACKMANN, D. E., MLADEJOUSKY, M., and PARKIN, J. L. (1988): 'Auditory prosthesis research with multiple channel intracochlear stimulation in man', *Ann. Otol. Rhinol. Laryngol. Suppl.*, **87**, pp. 5–39

ENGSTRÖM, H., ADES, H.W., and BREDBERG, G. (1970): 'Normal structure of the organ of Corti and the effect of noise-induced cochlear damage' in WOLSTENHOLME, G. E. W. and KNIGHT, J. (Eds): '*Sensorineural hearing loss*' (J. & A. Churchill, London, 1970)

FINLEY, C. C., WILSON, B. S., and WHITE, M. W. (1990): 'Models of neural responsiveness to electrical stimulation', in MILLER, J. M. and SPELMAN, F. A. (Eds): '*Cochlear implants*' (Springer-Verlag Inc., New York, 1990), pp. 55–96

FRIJNS, J. H. M., DE SNOO, S. L., and SCHOONHOVEN, R. (1995): 'Potential distributions and neural excitation patterns in a rotationally symmetric model of the electrically stimulated cochlea', *Hearing Res.*, **87**, pp. 170–186

FRIJNS, J. H. M., DE SNOO, S. L., and TEN KATE, J. H. (1996): 'Spatial selectivity in a rotationally symmetric model of the electrically stimulated cochlea', *Hearing Res.*, **95**, pp. 33–38

FRIJNS, J. H. M., BRIAIRE, J. J., DE LAAT, J. A. P. M., and GROTE, J. J. (2002): 'Initial evaluation of the Clarion CII cochlear implant: Speech perception and neural response imaging', *Ear Hearing*, **23**, pp. 184–197

GRILL, W. M., and MORTIMER, J. T. (1994): 'Electrical properties of implant encapsulation tissue', *Ann. Biomed. Eng.*, **22**, pp. 23–33

GSTOETTNER, W., ADUNKA, O., FRANZ, P., HAMZAVI, J., PLENK, H. JR., SUSANI, M., BAUMGARTNER, W., and KIEFER, J. (2001): 'Perimodiolar electrodes in cochlear implant surgery', *Acta Otolaryngologica*, **121**, 216–219

HANEKOM, T. (2001): 'Three-dimensional spiraling finite element model of the electrically stimulated cochlea', *Ear Hearing*, **22**, pp. 300–315

JOLLY, C. N., CLOPTON, B. M., SPELMAN, F. A., and LINEAWEAVER, S. K. (1997): 'Guinea pig auditory nerve response triggered by a high density electrode array', *Med. Progr. Technol.*, **21**, pp. 13–23

KAWANO, A., SELDON, H. L., CLARK, G. M., RAMSDEN, R. T., and RAINE, C. H. (1998): 'Intracochlear factors contributing to psychophysical percepts following cochlear implantation', *Acta Oto-Laryngologica*, **118**, pp. 313–326

KESSLER, D. K. (1999): 'The Clarion multi-strategy cochlear implant', *Ann. Otol., Rhinol. Laryngol.*, **108**, pp. 8–16

LEAKE, P. A., SNYDER, R. L., HRADEK, G. T., and REBSCHER, S. J. (1992): 'Chronic intracochlear electrical stimulation in neonatally deafened cats: Effects of intensity and stimulating electrode location', *Hearing Res.*, **64**, pp. 99–117

LINTHICUM, F. H. JR., FAYAD, J., OTTO, S. R., GALEY, F. R., and HOUSE, W. F. (1991): 'Cochlear implant histopathology', *Am. J. Otol.*, **12**, pp. 245–311

MILLER, A. L., MORRIS, D. J., and PFINGST, B. E. (2000): 'Effects of time after deafening and implantation on guinea pig electrical detection thresholds', *Hearing Res.*, **144**, pp. 175–186

NANAS, N. N. (1988): 'Biocompatibility overview: Classes of materials, inflammation, infection', in WEBSTER, J. G. (Ed.): '*Encyclopedia of medical devices and instrumentation*' (Wiley, 1988), pp. 181–194

PFINGST, B. E. (1990): 'Changes over time in thresholds for electrical stimulation of the cochlea', *Hearing Res.*, **50**, pp. 225–236

REILLY, J. P., FREEMAN, V. T., and LARKIN, W. D. (1985): 'Sensory effects of transient electrical stimulation. Evaluation with a neuroelectric model', *IEEE Trans. Biomed. Eng.*, **32**, pp. 1001–1011

SELDON, H. L., DAHM, M. C., CLARK, G. M., and CROWE, S. (1994): 'Silastic with polyacrylic acid filler: Swelling properties, biocompatibility and potential use in cochlear implants', *Biomaterials*, **15**, pp. 1161–1169

SHEPHERD, R. K., HATSUSHIKA, S.-I., and CLARK, G. M. (1993): 'Electrical stimulation of the auditory nerve. The effect of electrode position on neural excitation', *Hearing Res.*, **66**, pp. 108–120

SKINNER, M. W., KETTEN, D. R., VANNIER, M. W., GATES, G. A., YOFFIE, R. L., and KALENDER, W. A. (1994): 'Determination of the position of Nucleus cochlear implant electrodes in the inner ear', *Am. J. Otol.*, **15**, pp. 644–651

SPELMAN, F. A., PFINGST, B. E., MILLER, J. M., HASSUL, M., and POWERS, W. E. (1980): 'Biophysical measurements in the implanted cochlea', *Oto-Laryngol.: Head-Neck Surg.*, **88**, pp. 183–187

SPELMAN, F. A., CLOPTON, B. M., and PFINGST, B. E. (1982): 'Tissue impedance and current flow in the implanted ear. Implications for the cochlear prosthesis', *Ann. Otol. Rhinol. Laryngol. Suppl. (United States)*, **91**, pp. 3–8.

SPELMAN, F. A., CLOPTON, B. M., CLARY, T., CORBETT, S., JOLLY, C. N., VOIE, A. H., RODENHISER, K. L., and LINEAWEAVER, S. K. (1996): 'Potential field focussing and the design of cochlear electrode arrays'. 18th Ann. Int. Conf. IEEE EMBS, Amsterdam, pp. 329–330

SPOENDLIN, H., and SCHROTT, A. (1989): 'Analysis of the human auditory nerve', *Hearing Res.*, **43**, pp. 25–38

TYE-MURRAY, N., TYLER, R. S., WOODWORTH, G. G., and GANTZ, B. J. (1992): 'Performance over time with Nucleus or Ineraid cochlear implant', *Ear Hearing*, **13**, pp. 200–209

TYKOCINSKI, M., SAUNDERS, E., COHEN, L. T., TREABA, C. G., BRIGGS, R. J. S., GIBSON, P., CLARK, G. M., and COWAN, R. S. (2001): 'The Contour electrode array: Safety study and initial patient trials of a new perimodiolar design', *Otol. Neurotol.*, **22**, pp. 33–41

WEBB, R. L., CLARK, G. M., SHEPHERD, R. K., FRANZ, B. K., and PYMAN, B. C. (1988): 'The biological safety of the Cochlear Corporation multiple-electrode intracochlear implant', *Am. J. Otol.*, **9**, pp. 8–13

YOUNG, N. M., and GROHNE, K. M. (2001): 'Comparison of pediatric Clarion recipients with and without the electrode positioner', *Otol. Neurotol.*, **22**, pp. 195–199

ZAPPIA, J. J., NIPARKO, J. K., OVIAT, D. L., KEMINK, J. L., and ALTSCHULER, R. A. (1991): 'Evaluation of the temporal bones of a multichannel cochlear implant patient', *Ann. Otol. Rhinol. Laryngol.*, **100**, pp. 914–921

ZWICKER, E., and FASTL, H. (1990): '*Psychoacoustics: Facts and models*' (Springer-Verlag, Berlin, Heidelberg, 1990)

Author's biography

TANIA HANEKOM graduated in 1993 with a BEng degree in Electronic Engineering from the University of Pretoria. She completed a Masters degree in Electronic Engineering (with honours) in 1996 and a PhD degree in Engineering in 2001, all from the University of Pretoria, South Africa. Her research interests include modelling of electrical fields in biological systems, modelling of physiological systems, cochlear implants and biomaterials. She is currently a senior lecturer in the Department of Electrical, Electronic and Computer Engineering at the University of Pretoria.